Volume 16 | Number 13 | 7 April 2014 | Pages 5877–6304

PCCP

Physical Chemistry Chemical Physics

www.rsc.org/pccp

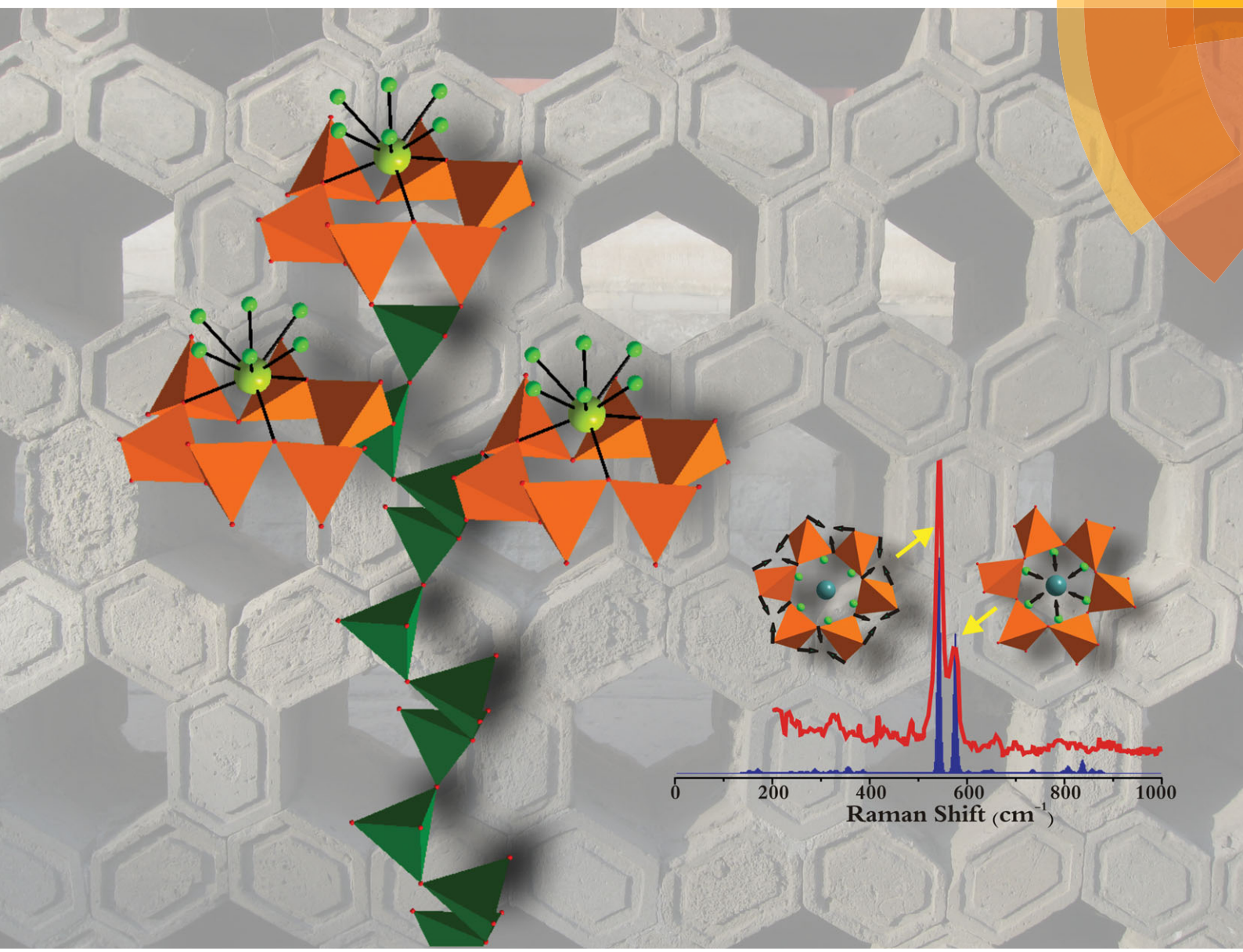

ISSN 1463-9076

ROYAL SOCIETY OF CHEMISTRY

PAPER

Xia, Atuchin *et al.*

Crystal and local structure refinement in $Ca_2Al_3O_6F$ explored by X-ray diffraction and Raman spectroscopy

PCCP

PAPER

View Article Online
View Journal | View Issue

Crystal and local structure refinement in $Ca_2Al_3O_6F$ explored by X-ray diffraction and Raman spectroscopy†

Cite this: *Phys. Chem. Chem. Phys.*, 2014, **16**, 5952

Zhiguo Xia,*[a] Maxim S. Molokeev,[b] Aleksandr S. Oreshonkov,[c] Victor V. Atuchin,*[d] Ru-Shi Liu[e] and Cheng Dong[f]

Received 8th September 2013,
Accepted 30th October 2013

DOI: 10.1039/c3cp53816h

www.rsc.org/pccp

We present a combined structural analysis on the powder of the $Ca_2Al_3O_6F$ phase using X-ray diffraction (XRD) and Raman spectroscopy techniques. The crystal structure of $Ca_2Al_3O_6F$ has been refined in the rhombohedral system, $R\bar{3}$ space group, a = 17.3237(7) Å, c = 7.00017(4) Å, V = 1819.38(2) Å^3, Z = 6. The $Ca_2Al_3O_6F$ phase consists of almost ideal AlO_4 tetrahedrons linked through corners, Ca^{2+} ions in voids, and F^- ions disordered over 6 sites around the Ca2 ion. The two different Ca sites have also been verified by the photoluminescence spectrum and decay curves using Eu^{2+} as the probe ion substituted onto the Ca^{2+} sites. A lattice dynamics simulation based on the simplified version of the Born–Karman potential model has been produced. Calculated Raman phonon modes agree qualitatively well with the experimental data. The calculations show that the strong line at 538 cm^{-1} (A_g) corresponds to the vibrational mode of a six-membered AlO_4 tetrahedrons ring, and the line at 572 cm^{-1} (A_g) corresponds to the full symmetric vibration of fluorine atoms in the *ab* crystal plane.

1. Introduction

The incorporation of halogen ions into an oxide crystal lattice leads to a competition between anions for the valence electrons of metal ions. This results in pronounced distortion of the coordination polyhedrons, anion disordering and sequent phase transitions on temperature variation, bond ionicity variation and other effects common in oxyhalogenides.[1–5] Due to these effects, oxyhalogenides possess a pronounced ability for the generation of non-centrosymmetric structures, accommodation of doping elements, specific electronic structure and unusual spectroscopic properties that gives a potential for the creation of new technologically important multifunctional materials with ferroelectric, luminescent, electrochemical and non-linear optical properties.[6–12] In comparison to other oxyhalogenides, the oxyfluorides are of special interest because effective ionic radii of O^{2-} and F^- ions are comparable and the stable anionic sublattice can be formed at different O/F ratios.[13] Many oxyfluorides with valuable properties and high chemical stability in the air environment have been discovered in the past. In particular, oxyfluorides can be found as the efficient phosphor hosts in some references.[14]

Recently, interesting luminescence properties were also found in $Ca_2Al_3O_6F$ oxyfluoride activated with rare-earth ions by our research group.[15,16] This compound was firstly detected in the $CaO–Al_2O_3–CaF_2$ ternary system and reported as being hexagonal with unit cell parameters a = 17.29 Å and c = 7.01 Å.[17] As for physical properties, density, melting point and refractive indices were measured using a $Ca_2Al_3O_6F$ occasionally found in experiments with aluminous cements. Commonly, an admixture of $Ca_2Al_3O_6F$ can be found in $CaO–Al_2O_3–CaF_2$ slags with different compositions.[17,18] The crystal structure of $Ca_2Al_3O_6F$, however, remains to be unknown although it has been proposed as an efficient host for luminescent materials. Therefore, the present study aims to produce a complex evaluation of the crystal and local structure of the $Ca_2Al_3O_6F$ oxyfluoride by X-ray diffraction methods and Raman spectroscopy. Based on the present study, it is expected that the combined physical and chemical methods to resolve the crystal structure and local structure of the new inorganic phase will be established, which will be helpful to understand the new functional materials and develop new applications.

[a] *School of Materials Sciences and Technology, China University of Geosciences, Beijing 100083, China. E-mail: xiazg@cugb.edu.cn; Fax: +86-10-8232-2974; Tel: +86-10-8233-2247*
[b] *Laboratory of Crystal Physics, Kirensky Institute of Physics, SB RAS, Akademgorodok, Krasnoyarsk, 660036, Russia*
[c] *Laboratory of Molecular Spectroscopy, Kirensky Institute of Physics, SB RAS, Akademgorodok, Krasnoyarsk, 660036, Russia*
[d] *Laboratory of Optical Materials and Structures, Institute of Semiconductor Physics, SB RAS, Novosibirsk 90, 630090, Russia. E-mail: atuchin@isp.nsc.ru; Fax: +7 383 3332771; Tel: +7 383 3308889*
[e] *Department of Chemistry, National Taiwan University, Taipei 10617, Taiwan*
[f] *Institute of Physics, Chinese Academy of Sciences, Beijing 100190, China*

† Electronic supplementary information (ESI) available: CIF file of $Ca_2Al_3O_6F$ phase, Table S1, A_g (797 cm^{-1}) vibrational mode of AlO_4 tetrahedrons, A_g (252 cm^{-1}) vibrationalesi mode of fluorine in $Ca_2O_3F_4$ polyhedrons. See DOI: 10.1039/c3cp53816h

2. Experimental methods

The $Ca_2Al_3O_6F$ polycrystalline powder was prepared by a conventional solid-state reaction from high-purity (>99.95%) starting materials of $CaCO_3$, Al_2O_3, and CaF_2, which were all purchased from the Beijing Chemical Company, China. In a typical procedure, all the starting materials were weighted according to the given stoichiometric ratio except for some excessive CaF_2 (5 wt%) and the corresponding decreased $CaCO_3$, which was necessary to compensate for the fluorine loss at high temperatures. After this, the reagents were mixed and carefully ground in an agate mortar. Then the prepared charge was placed into an alumina crucible and was fired at 1250 °C for 4 h. It was found that a higher temperature (>1250 °C) and longer synthesis time (>4 h) are dangerous to give a loss of the fluorine component, which in turn induces deviations of the phase and chemical composition. After the heat treatment, the sample was furnace-cooled to room temperature and ground again up to fine powder suitable for structural analysis and spectroscopic measurements.

Powder X-ray diffraction data were collected on a Rigaku Ultima IV diffractometer using Cu-Kα radiation operating at 40 kV and 40 mA. The beam was controlled by a 0.5° fixed divergence slit and a 5 mm receiving slit. The diffraction data were collected using the high-speed D/teX Ultra detector in 0.02° steps over the wide 2θ range of 3–139° with a scan speed of 1° min^{-1}. The cell parameters and space group were found using the program DASH 3.3 and the program TOPAS 4.2.[19,20]

The room temperature emission spectrum was measured on a Hitachi F4600 fluorescence spectrophotometer with a photomultiplier tube operating at 400 V, and a 150 W Xe lamp was used as the excitation source. The decay curves were recorded on a JOBIN YVON FL3-21 spectrofluorometer, and the 370 nm pulse laser radiation (nano-LED) was used as the excitation source. The Raman spectrum was measured on a PerkinElmer Flex-400 device (laser wavelength = 785.14 nm, power = 80 mW, CCD dimensions: 1024 × 255) at a temperature of $T = -50$ °C.

3. Computational methods

The vibrational representation for the rhombohedral phase at the Brillouin zone center is:

$$\Gamma_{vibr} = 25A_{1g} + 25E_g + 25A_u + 25E_u \quad (1)$$

Acoustic and optic modes:

$$\Gamma_{acoustic} = A_u + E_u \quad (2)$$

$$\Gamma_{optic} = 25A_{1g} + 25E_g + 24A_u + 24E_u \quad (3)$$

Infrared and Raman active modes:

$$\Gamma_{infrared} = 24A_u + 24E_u \quad (4)$$

$$\Gamma_{Raman} = 25A_{1g} + 25E_g \quad (5)$$

To calculate the $Ca_2Al_3O_6F$ vibrational spectrum, the program package LADY was used.[21] A simplified version of the Born–Karman model was explored to define the atomic vibrations.[22] In this approximation, the pair-wise atomic interactions are considered and only bond-stretching force constants $A = \frac{\partial^2 E}{\partial R^2}$ (E – energy, R – bond length) are taken into account. The simplified version of the Born–Karman model implies that A level is dependent on R and the $A(R)$ functions are the same for all atom pairs:

$$A = \lambda \exp(-r_{ij}/\rho), \quad (6)$$

where r_{ij} is the interatomic distance and λ and ρ are the parameters characterizing the pair interaction. To find the parameters of the model, an optimization program was written and tested previously for several crystals.[23] The lattice stability conditions were taken into account. The model parameters used in eqn (6) can be found in Table S1 (ESI†).

The lattice vibration calculation consists of an evaluation and diagonalization of the dynamic matrix D_{ij}:

$$D_{ij} = \frac{1}{\sqrt{m_i m_j}} V_{ij}^{xx} \rightarrow \sum_j D_{ij} h_{jn} = \lambda_n h_{in} \quad (7)$$

where V_{ij}^{xx} are the atomic force constants. Thus, the eigenvalues λ_n and eigenvectors h_{in} were determined that enable the phonon frequencies

$$w_n = \sqrt{\lambda_n} \quad (8)$$

and the corresponding atomic displacements (mass-weighted eigenvectors)

$$e_{in} = \frac{1}{\sqrt{m_i}} h_{in} = \frac{dx_i}{dQ_n} \quad (9)$$

to be obtained. An expression for the Raman scattering intensity is given by

$$\zeta_n = \sum_i \varepsilon_i^{\infty} e_{in} \quad (10)$$

where $\varepsilon_i^{\infty} = \frac{d\varepsilon^{\infty}}{dx_i}$ are atomic derivatives of the dielectric constant.

4. Results and discussion

The structural analysis reveals that the $Ca_2Al_3O_6F$ crystal is trigonal with unit cell parameters a = 17.305 Å, c = 6.9925 Å. The most probable space groups are $R3$, $R\bar{3}$, $R3m$, $R32$ and $R\bar{3}m$. Therefore, the structure solving in these two lowest point groups, $R3$ and $R\bar{3}$, will account for all possible solutions in higher point groups. The program TOPAS 4.2 was used to solve and refine the crystal structure. Initially, it was decided to solve the structure in the $R\bar{3}$ space group. It was solved using a simulated annealing procedure applied to the randomized coordinate and orientation of two AlO_4 tetrahedrons and two Ca ions. The dynamical occupancy correction of the atoms was used to merge the tetrahedrons and adjust the occupancy of atoms falling in a special position.[24,25] After the calculations, a solution was found with R_{wp} = 16.3%. Then, the simulated annealing procedure was applied to the F atom. Other atoms were constrained. Finally, atom F was localized in the18f Wyckoff position near Ca2 and R_{wp} = 13.8% was achieved.

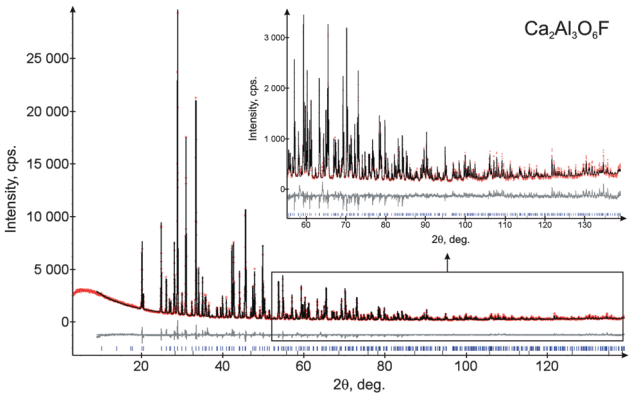

Fig. 1 X-ray diffraction pattern of $Ca_2Al_3O_6F$.

The chemical sum formula of $Ca_2Al_3O_6F$ requires the occupancy of two-thirds of the 18 sites used by fluorine atoms. One can see that atom F is disordered in structure. The refinement of this crystal structure with the isotropic thermal parameters of all atoms was stable and gave a low R_B factor and R_{wp} = 7.38% (Fig. 1). The main parameters of refinement are given in Table 1. The impurity of residual CaF_2 was detected and relative phase amounts in the mixture were refined. It was found that the components of $Ca_2Al_3O_6F$ and CaF_2 are 98.6(1)% and 1.4(1)% in the mixture, respectively. The structural analysis of $Ca_2Al_3O_6F$ using the program PLATON did not reveal additional elements of symmetry.[26] Therefore, the $R\bar{3}$ space group was chosen correctly, and the selection for $R\bar{3}$ is ideal for this structure and there is no reason to increase symmetry. Further details of the crystal structure may be obtained from Fachinformationszentrum Karlsruhe on quoting the deposition number CSD-426334 and the supporting information containing the CIF file.[27] The coordinates of atoms in $Ca_2Al_3O_6F$, space group $R\bar{3}$, are given in Table 2.

The crystal structure of $Ca_2Al_3O_6F$ is shown in Fig. 2 in the projection of the unit cell on the *ab* plane. The structure consisted of almost ideal AlO_4 tetrahedrons linked through the corners, the Ca^{2+} ions are in voids, and the F^- ions are disordered over one site and 6 sites around the Ca1 and Ca2 ions, respectively. Only two tetrahedrons are linked in each node. The corner-linked Al1 tetrahedrons form six-membered rings as shown in Fig. 2 and 3. The Ca2 ion is in the center of the ring and has a special 6c position on $\bar{3}$-fold axis. The Ca1 ion is in the general 18f position. The Al2 tetrahedrons linked through

Table 1 Main parameters of crystal structure refinement

Space group	$R\bar{3}$
a_i, Å	17.3237(7)
c_i, Å	7.00017(4)
V, Å^3	1819.38(2)
Z	6
2θ-interval, °	9–139
Number of reflections	772
Number of parameters of refinement	62
R_{wp},%	7.380
R_p,%	5.296
R_{Bragg},%	3.445
χ	1.971

Table 2 Fractional atomic coordinates and isotropic or equivalent isotropic displacement parameters (Å^2)

	x	y	z	B_{iso}*/B_{eq}	Occ. (<1)
Ca1	0.22316 (10)	0.41486 (10)	0.0760 (2)	2.24 (5)	
Ca2	0	0	0.2771 (4)	2.63 (8)	
Al1	0.59279 (16)	0.45660 (17)	0.2984 (3)	1.85 (6)	
Al2	0.64325 (17)	0.05015 (16)	0.1027 (4)	1.82 (6)	
O1	0.5943 (3)	0.5403 (3)	0.4458 (6)	1.57 (11)	
O2	0.1400 (3)	0.1113 (3)	0.1173 (6)	2.59 (13)	
O3	0.5582 (3)	0.0773 (3)	0.1175 (6)	2.16 (11)	
O4	0.6009 (3)	−0.0578 (3)	0.1941 (6)	1.98 (12)	
F	0.3411 (8)	0.5681 (6)	0.1799 (12)	7.6 (3)	0.6667

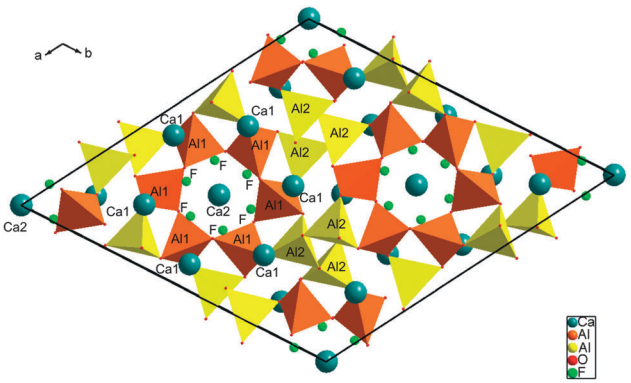

Fig. 2 The crystal structure of $Ca_2Al_3O_6F$, and the unit cell is outlined.

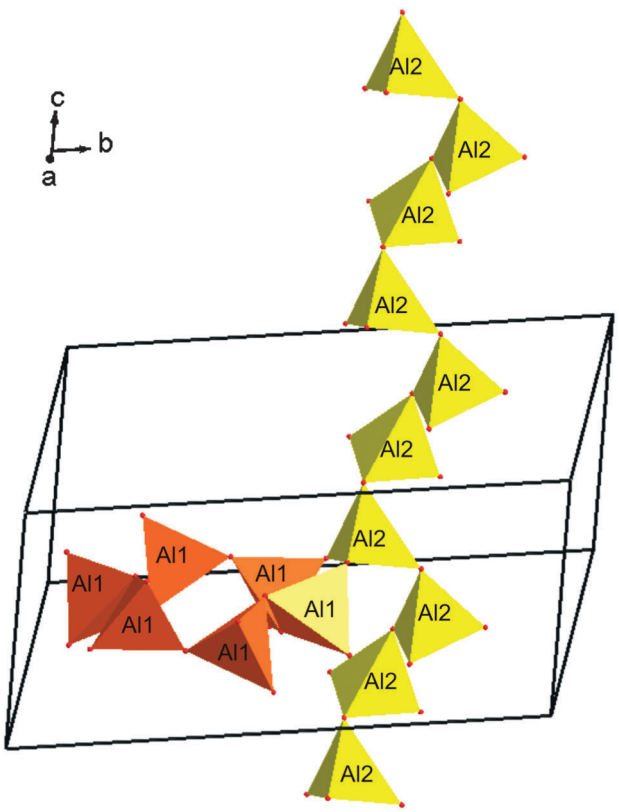

Fig. 3 The helicoid formed by Al2 tetrahedrons and the six-membered ring formed by Al1 tetrahedrons.

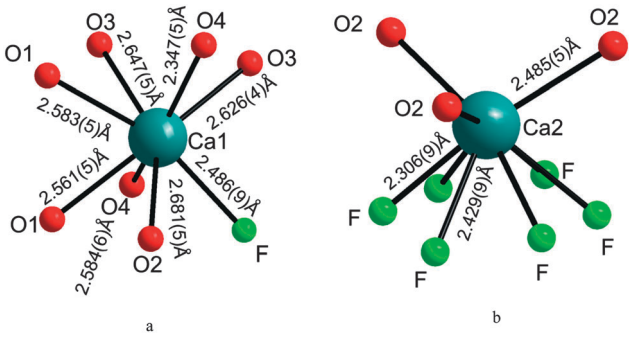

Fig. 4 (a) Ca1 coordination; (b) Ca2 coordination.

corners form a helix along the *c*-axis, as shown in Fig. 3. The helices and six-membered rings are linked each other and form a 3d-network. Since the Ca1 and Ca2 ions are independent, they have distinct coordination as shown in Fig. 4. Ca1 forms a square antiprism (Fig. 4a), and Ca2 forms the polyhedron with 9 nodes where 6 nodes are occupied on 2/3 by the F^- ions (Fig. 4b). All *d*(Ca–O) bond lengths are in the range of 2.098–2.86 Å that is well related to the conventional Ca–O bond length range in pure oxides.[28] Two *d*(Ca–F) bond lengths found in $Ca_2Al_3O_6F$ are slightly above the maximum Ca–F bond length 2.362 Å recommended by the International Tables.[28] This difference may be interpreted as evidence that the structure should be properly described in terms of a lower space group. But the refinement of structure in the asymmetric *R*3 space group was unstable and gave worse *R*-factors. The complex anion sublattice and partial F position occupancy, on the other hand, may be the factors inducing the *d*(Ca–F) value above the range of *d*(Ca–F) in pure fluorides. As an example, in the structure of $Ca_6Al_7O_{16}F$, due to Ca and F disorder, the *d*(Ca–F) bond lengths are reported to be in the range of 2.31–2.82 Å.[29] Evidently, atom disorder complicates the bond length analysis, and, moreover, partial occupancy of light atom positions leads to an inaccuracy of their coordinate determination. The high thermal parameter of F also indicates that the model of disorder is more complex than that considered in the present refinement. As to Al–O bonding, all bond lengths *d*(Al–O) in the structure are in the range of 1.724–1.782 Å, which is typical for most Ca–Al–O structures.[29–32]

In order to further demonstrate the details of the crystal structure of $Ca_2Al_3O_6F$, especially the Ca site coordination information, Eu^{2+} was selected as a probe ion by occupying the Ca^{2+} sites, as reported in our previous work.[15] Fig. 5a shows the photoluminescence (PL) spectrum of $Ca_{1.95}Al_3O_6F{:}0.05Eu^{2+}$ phosphor upon excitation at 400 nm. Previously, we considered that only one emission center exists in this phosphor, however, two obvious Gaussian type profiles can be fitted by careful analysis and two bands centered at 489 nm and 511 nm can be distinguished, as given in Fig. 5a. The two possible emission centers also remains consistent with the above crystal structure analysis. Furthermore, the emission wavelength dependent decay curves have been recorded from 480 to 520 nm (except for the observed emission center of 501 nm) with a step of 10 nm,

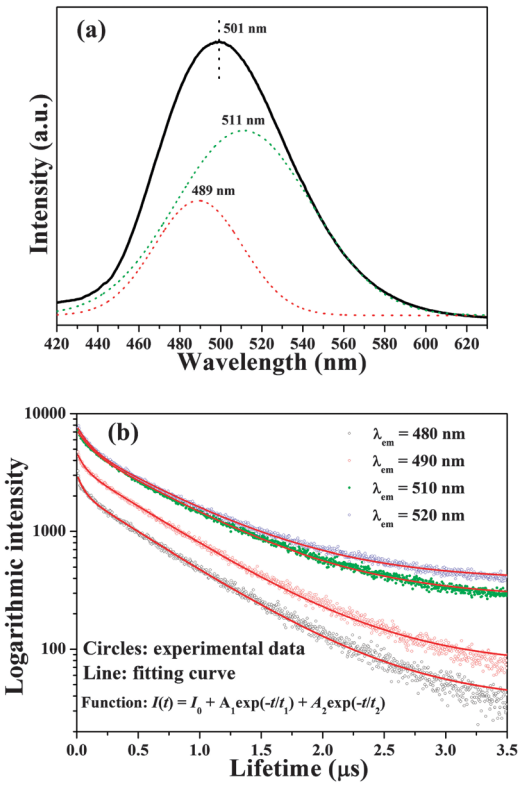

Fig. 5 (a) The PL (λ_{ex} = 400 nm) spectrum of $Ca_{1.95}Al_3O_6F{:}0.05Eu^{2+}$; (b) decay curves of $Ca_{1.95}Al_3O_6F{:}0.05Eu^{2+}$ with different monitoring wavelengths.

as shown in Fig. 5b. It has been found that all the experimental data can be fitted by the biexponential equation given by the following expression:[33]

$$I = A_1\exp(-t/\tau_1) + A_2\exp(-t/\tau_2) \quad (11)$$

where *I* is the luminescence intensity at time *t*, A_1 and A_2 are constants, and τ_1 and τ_2 are the decay times of individual exponential components. Moreover, the average lifetime (τ^*) can be determined using the formula:

$$\tau^* = (A_1\tau_1^2 + A_2\tau_1^2)/(A_1\tau_1 + A_2\tau_1) \quad (12)$$

On the basis of eqn (11) and (12), the average lifetime of Eu^{2+} at different wavelengths was defined to be 0.62, 0.63, 0.68 and 0.68 μs for the monitoring emission wavelengths of 480, 490, 510 and 520 nm, respectively. The biexponential decay behavior verifies the possibility of two different emission centers, and the obtained lifetime can also be divided into two groups of emission centers which should be ascribed to the two different Ca sites with strong differences in the chemical environment: Ca1 is coordinated by 7O and 1F occupied on 2/3, while Ca2 is 7-fold coordinated by 3O and 4F with disorder accounting, as shown in Fig. 4.

Raman spectroscopic analysis plays an important role in the understanding the local structure of inorganic compounds. Therefore, structures and vibrations of some typical aluminates represented by $CaAl_2O_4$ and the fluorapatite with "free" F atoms ($Ca_{10}(PO_4)_6F_2$), which are partially similar to the structure of the

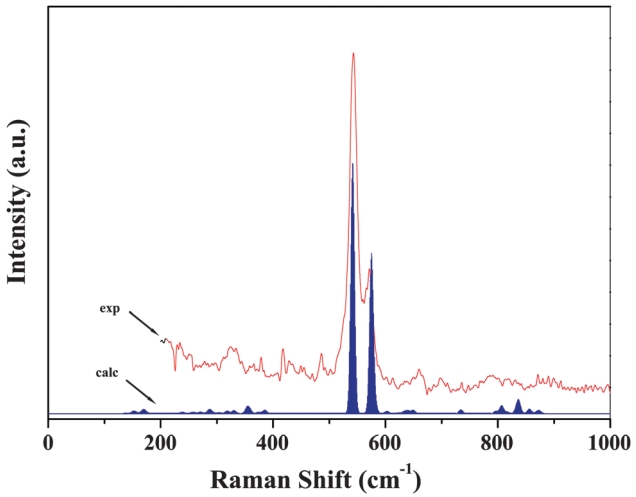

Fig. 6 The experimental and calculated Raman spectra of the as-prepared $Ca_2Al_3O_6F$.

present $Ca_2Al_3O_6F$, have been taken into account in order to compare with the findings here.[34] The experimental and calculated Raman spectra in $Ca_2Al_3O_6F$ are compared in Fig. 6. The parameters of the calculated Raman lines are presented in Table 3. Only two strong Raman lines at 538 and 572 cm^{-1} were recorded from the $Ca_2Al_3O_6F$ powder sample, which have similar results to some previous reports.[35] This result is well related to the theoretical spectrum where only two intensive lines were found in combination with a suite of numerous low-intensity vibrations at frequencies of 600–870 cm^{-1} and <400 cm^{-1}. As is shown by the theoretical analysis, the symmetry and frequency of these most intensive vibrations in the Raman spectra are: A_g = 538 cm^{-1} and

Table 3 Calculated Raman line wavenumbers in $Ca_2Al_3O_6F$

Raman (cm^{-1})	
A_g	E_g
133	122
140	139
150	149
160	154
180	176
191	194
210	212
219	231
238	248
247	266
271	282
282	308
296	321
343	345
366	349
397	376
538	574
572	598
577	625
615	640
632	733
797	806
834	816
857	837
867	873

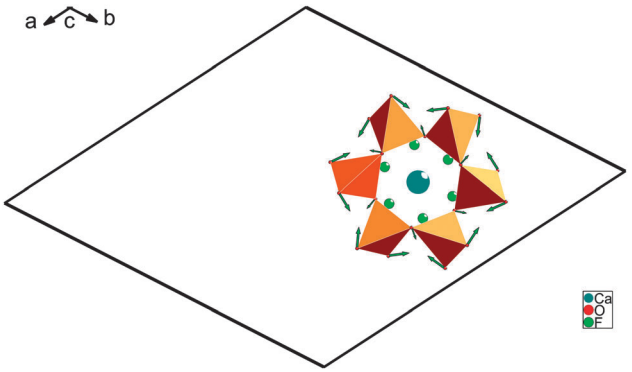

Fig. 7 A_g (538 cm^{-1}) vibrational mode of the six-membered AlO_4 tetrahedron ring.

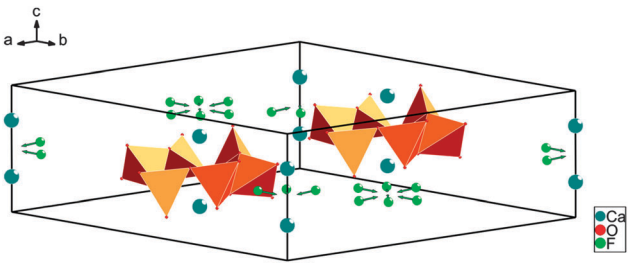

Fig. 8 A_g (572 cm^{-1}) vibrational mode of fluorine atoms in the *ab* crystal plane. Only the Ca2 atoms are shown for clarity.

A_g = 572 cm^{-1}. The line at 538 cm^{-1} corresponds to the vibrational mode of the six-membered AlO_4 tetrahedron ring as shown in Fig. 7, and the line at 572 cm^{-1} appears due to the full symmetric vibration of fluorine atoms in the *ab* crystal plane, as it is depicted in Fig. 8. The intensity of the Raman peaks depends in a complex way on the concentration of the active species and, as we can see in eqn (10), it is also dependent on the atomic displacement and atomic derivatives of the dielectric constant. The calculations show that the atomic displacements corresponding to the lines at 538 and 572 cm^{-1} in the Raman spectra are much more intensive in magnitude than the atom displacements corresponding to other Raman lines. Frequency differentiation was used to elucidate the microscopic origin of vibrational states in other parts of the Raman spectrum.[21] In $Ca_2Al_3O_6F$, the full spectrum could be subdivided to two parts, namely, the low-frequency region of the Raman spectrum of <400 cm^{-1} related to mixed vibrations appeared due to the Ca–O and Ca–F pair interactions and high-frequency region of AlO_4 vibrations over the range of 600–870 cm^{-1}. As an example of high-frequency vibrations, the internal A_g vibrations of the AlO_4 tetrahedrons at $\sim$797 cm^{-1} are shown in Fig. S1 (ESI†). As for the low-frequency vibrations, the A_g-type vibrations of fluorine atoms in $Ca_2O_3F_4$ polyhedrons at 252 cm^{-1} are depicted in Fig. S2 (ESI†).

5. Conclusions

We successfully prepared the $Ca_2Al_3O_6F$ phase, and the crystal structure has been refined in the rhombohedral system,

space group $R\bar{3}$, $a = 17.3237(7)$ Å, $c = 7.00017(4)$ Å, $V = 1819.38(2)$ Å^3, $Z = 6$. The $Ca_2Al_3O_6F$ structure is formed by almost ideal AlO_4 tetrahedrons linked through the corners, the Ca^{2+} ions in voids, and the F^- ions disordered over one site and 6 sites around the Ca1 and Ca2 ions, respectively. The presence of two different Ca sites has also been verified by the photoluminescence measurements and the corresponding dynamic analysis. The relationship between the calculated phonon modes of the AlO_4 tetrahedrons, the six-membered AlO_4 tetrahedrons ring, and the F atoms on the *ab* crystal plane in the $Ca_2O_3F_4$ polyhedrons and the observed Raman spectra has been built up, and all of them have been used to understand the local structure of $Ca_2Al_3O_6F$. The present result indicates that the combination of X-ray diffraction techniques and vibrational spectroscopy is a useful tool to reveal fine structural information on new solid materials.

Acknowledgements

This present work was supported by the National Natural Science Foundations of China (Grant No. 51002146, 51272242), Natural Science Foundations of Beijing (2132050), the Program for New Century Excellent Talents in University of Ministry of Education of China (NCET-12-0950), Beijing Nova Program (Z131103000413047) and Beijing Youth Excellent Talent Program (YETP0635), and this study was also partially supported by SB RAS, Grant 28.13. Part of the work was supported by the National Science Council of Taiwan under contract No. NSC 101-2113-M-002-014-MY3.

References

1 M. R. Marvel, J. Lesage, J. Baek, H. Stern, P. Shiv Halasyamani, C. L. Stern and K. R. Poeppelmeier, *J. Am. Chem. Soc.*, 2007, **129**, 13963–13969.
2 M. R. Marvel, R. A. F. Pinlac, J. Lesage, C. L. Stern and K. R. Poeppelmeier, *Z. Anorg. Allg. Chem.*, 2009, **635**, 869–877.
3 R. K. Li and P. Chen, *Inorg. Chem.*, 2010, **49**, 1561–1565.
4 M. S. Molokeev, S. V. Misyul, V. D. Fokina, A. G. Kocharova and K. S. Aleksandrov, *Phys. Solid State*, 2011, **53**, 834–839.
5 V. V. Atuchin, M. S. Molokeev, G. Y. Yurkin, T. A. Gavrilova, V. G. Kesler, N. M. Laptash, I. N. Flerov and G. S. Patrin, *J. Phys. Chem. C*, 2012, **116**, 10162–10170.
6 V. D. Fokina, I. N. Flerov, M. V. Gorrev, M. S. Molokeev, A. D. Vasiliev and N. M. Laptash, *Ferroelectrics*, 2007, **347**, 60–64.
7 F. Sauvage, V. Bodenez, J. M. Tarascon and K. R. Poeppelmeier, *Inorg. Chem.*, 2010, **49**, 6461–6467.
8 Z. G. Xia, X. M. Wang, L. B. Liao and X. P. Jing, *Inorg. Chem.*, 2011, **50**, 10134–10142.
9 I. N. Flerov, M. V. Gorev, A. Tressaud and N. M. Laptash, *Crystallogr. Rep.*, 2011, **56**, 9–17.
10 M. Zhang, S. L. Pan, X. Y. Fan, Z. X. Zhou, K. R. Poeppelmeier and Y. Yang, *CrystEngComm*, 2011, **13**, 2899–2903.
11 V. V. Atuchin, L. L. Isaenko, V. G. Kesler, Z. S. Lin, M. S. Movokeev, A. P. Yelisseyev and S. A. Zhurkov, *J. Solid State Chem.*, 2012, **187**, 159–164.
12 Z. G. Xia, J. Q. Zhuang and L. B. Liao, *Inorg. Chem.*, 2012, **51**, 7202–7209.
13 R. D. Shannon and C. T. Prewitt, *Acta Crystallogr., Sect. B: Struct. Crystallogr. Cryst. Chem.*, 1969, **2**, 925–946.
14 W. B. Im, S. Brinkley, J. Hu, A. Mikhailovsky, S. P. DenBaars and R. Seshadri, *Chem. Mater.*, 2010, **22**, 2842–2849.
15 Z. G. Xia, R. S. Liu, K. W. Huang and V. J. Drozd, *J. Mater. Chem.*, 2012, **22**, 15183–15189.
16 Z. G. Xia and R. S. Liu, *J. Phys. Chem. C*, 2012, **116**, 15604–15609.
17 J. K. Leary, *Nature*, 1962, **4823**, 79–80.
18 K. W. Peng, P. Zhang, J. G. Xie and H. L. Ma, *PTS 1-3 Book Series: Applied Mechanics and Materials*, 2012, vol. 117–119, pp. 269–272.
19 V. Favre-Nicolin and R. Cerny, *J. Appl. Crystallogr.*, 2006, **39**, 910–915.
20 Bruker AXS (2008): TOPAS V4: General Profile and Structure Analysis Software for Powder Diffraction Data. – User's Manual, Bruker AXS, Karlsruhe, Germany, 2008.
21 M. B. Smirnov and V. Y. Kazimirov, LADY: Software for Lattice Dynamics Simulations. (JINR communications), E 14-2001-159, 2001.
22 M. Smirnov and R. Baddour-Hadjean, *J. Chem. Phys.*, 2004, **121**, 2348.
23 A. S. Krylov, S. N. Krylova, A. N. Vtyurin, V. N. Voronov and A. S. Oreshonkov, *Ferroelectrics*, 2012, **440**, 100–104.
24 V. Favre-Nicolin and R. Cerny, *Mater. Sci. Forum*, 2004, **443–444**, 35–38.
25 V. Favre-Nicolin and R. Cerny, *J. Appl. Crystallogr.*, 2002, **35**, 734–743.
26 PLATON – A Multipurpose Crystallographic Tool. Utrecht University, Utrecht, The Netherlands, 2008.
27 Fachinformationszentrum Karlsruhe, 76344 Eggenstein-Leopoldshafen, Germany (crystdata@fiz-karlsruhe.de; http://www.fiz-karlsruhe.de/request_for_deposited_data.html; +49-7247-808-666).
28 E. Prince, *International Tables for Crystallography*, *Volume C (Mathematical, Physical and Chemical Tables)*, Kluver Academic Publishers, 3rd edn, 2004, p. 1000.
29 P. P. Williams, *Acta Crystallogr., Sect. B: Struct. Crystallogr. Cryst. Chem.*, 1973, **29**, 1550–1551.
30 M. G. Vincent and J. W. Jeffery, *Acta Crystallogr., Sect. B: Struct. Crystallogr. Cryst. Chem.*, 1978, **34**, 1422–1428.
31 S. C. Abrahams and S. Geller, *Acta Crystallogr.*, 1958, **11**, 437–441.
32 V. I. Ponomarev, D. M. Heiker and N. V. Belov, *Kristallografiya*, 1970, **15**, 1140–1143.
33 G. Blasse and B. C. Grabmaier, *Luminescent Materials*, Springer-Verlag, Berlin, 1994.
34 C. Ma, A. R. Kampf, H. C. Connoll Jr, J. R. Beckett, G. R. Rossman, S. A. S. Smith and D. L. Schrader, *Am. Mineral.*, 2011, **96**, 709–715.
35 M. Ruszak, S. Witkowski, P. Pietrzyk, A. Kotarba and Z. Sojka, *Funct. Mater. Lett.*, 2011, **4**, 183–186.